Ab initio study of low-energy electron collisions with tetrafluoroethene C_2F_4

C. S. Trevisan,[1] A. E. Orel,[1] and T. N. Rescigno[2]
[1]*Department of Applied Science, University of California, Davis, California 95616, USA*
[2]*Lawrence Berkeley National Laboratory, Chemical Sciences, Berkeley, California 94720, USA*
(Received 2 March 2004; published 9 July 2004)

We report the results of variational calculations of elastic electron scattering by tetrafluoroethene (C_2F_4) with incident electron energies ranging from 0.5 to 20 eV, using the complex Kohn method and effective core potentials. These are the first fully *ab initio* calculations to reproduce experimental angular differential cross sections at energies below 10 eV. Low-energy electron scattering by C_2F_4 is sensitive to the inclusion of electronic correlation and target-distortion effects. We therefore present results that describe the dynamic polarization of the target by the incident electron. The calculated cross sections are compared with recent experimental measurements.

DOI: 10.1103/PhysRevA.70.012704 PACS number(s): 34.80.Gs

I. INTRODUCTION

Information regarding collisions of electrons with tetrafluoroethene (C_2F_4) is important in the plasma processing of semiconductors. C_2F_4 has attracted interest as a feed gas in plasma etching of the silicon oxide surface [1,2] and has been proposed as a new plasma reactant due to its low carbon-carbon bond strength and low global warming potential, with a consequent relatively benign impact on the atmosphere [3]. C_2F_4 is also formed within plasmas by dissociation of another common feed gas used for oxide etching, C_4F_8. In order to understand the role of collision processes in plasmas and their effects on plasma properties and dynamics, it is essential to have an in-depth knowledge of the physics of these processes and detailed information on their quantitative characteristics (transition rates, cross sections, reaction rates coefficients, etc.). Modeling of low-temperature plasmas requires the knowledge of a large number of cross sections involving electron-molecule interactions (electronic excitation, dissociation, and ionization).

There have been only very limited studies of the interaction of C_2F_4 with low-energy (<20 eV) electrons, both theoretically [4] and experimentally [5,6]. Winstead and McKoy [4] performed low-energy calculations using the Schwinger multichannel variational method. They reported low-energy differential and integrated cross sections for both electronically elastic and inelastic collisions. They found the elastic cross section to show a number of resonance features, which were classified according to symmetry and analyzed in relation to available experimental data. They did not, however, present elastic differential cross sections at electron energies below 10 eV.

Experimentally, Yoshida *et al.* [5] reported an analysis of electron swarm data together with theoretical estimates for elastic scattering and electronic excitation cross sections. Panajotovic *et al.* [6] performed experimental measurements utilizing two crossed-beam electron spectometers, one at Sophia University, Japan, and the other at the Australian National University. They reported cross sections between 1.5 and 100 eV. Significant differences in both magnitude and shape of cross sections can be seen between the swarm and crossed-beam studies, presumably due to missing vibrational intensity from the cross sections of Yoshida *et al.* [5,7].

The lack of information on low-energy electron scattering by this target and its growing importance in the low-temperature plasma environment has therefore led us to investigate elastic collisions of electrons with C_2F_4 in energy ranges between 0.5 and 20 eV. Low-energy electron scattering by atoms and molecules is sensitive to electrostatic interaction effects, electron exchange, and electron correlation. The proper inclusion of these factors is crucial for an accurate description of resonance parameters and vibrational excitation cross sections. We therefore present differential, integral, and momentum-transfer cross sections using the complex Kohn variational method, which will account for these low-energy effects. Our results are compared to the recent experimental measurements of Panajotovic *et al.* [6].

C_2F_4 is a closed-shell molecule which possesses a permanent quadrupole moment. C_2F_4 is isovalent with C_2H_4. Like C_2H_4, which we have recently studied [8], its electron collision cross sections show a Ramsauer-Townsend minimum in ^2A_g symmetry and a narrow shape resonance in $^2B_{2g}$ symmetry caused by the temporary capture of the incident electron into an empty, antibonding valence orbital. The C_2F_4 cross sections are also found to display resonance features in the symmetries ^2A_g, $^2B_{1u}$, and $^2B_{2u}$. The contribution of each individual symmetry (where these features can be observed more clearly) to the total elastic cross section is also reported in the present work.

II. THEORETICAL FORMULATION

A. Complex Kohn variational method

The complex Kohn method is a variational technique which uses a trial wave function that is expanded in terms of square-integrable (Cartesian Gaussian) and continuum basis functions that incorporate the correct asymptotic boundary conditions. Detailed descriptions of the method have been given in previous publications [9,10], so only a brief summary of the aspects that concern this study will be given below.

In the case of electronically elastic scattering, the trial wave function takes the form

$$\Psi = \mathcal{A}[\Phi_0(\vec{r}_1, \ldots, \vec{r}_N)F(\vec{r}_{N+1})] + \sum_\mu d_\mu \Theta_\mu(\vec{r}_1, \ldots, \vec{r}_{N+1}), \tag{1}$$

where Φ_0 is the (Hartree-Fock) ground state of C_2F_4, $\mathcal{A}$ antisymmetrizes the coordinates of the incident electron ($\vec{r}_{N+1}$) with those of the target, and the sum contains square-integrable, $(N+1)$-electron terms that describe polarization and/or correlation effects due to electronically closed channels. In the present study, these configuration-state functions (CSF's) Θ_μ were constructed by singly exciting the target Hartree-Fock wave function. Thus the configurations in Eq. (1) have the form

$$\Theta_\mu = \mathcal{A}(\Phi_0[\phi_0 \rightarrow \phi_\alpha]\phi_i), \tag{2}$$

where $\phi_0 \rightarrow \phi_\alpha$ denotes the replacement of occupied orbital ϕ_0 by orbital ϕ_α, and ϕ_i is another virtual orbital.

The proper construction of the correlation component of the trial wave function is critical in determining the low-energy behavior of the elastic cross sections and the position and width of shape resonances. The nature of this correlation and, consequently, the way it is modeled depend on the details of the target molecule and the symmetry under consideration. These different approaches will be described throughout the sections that follow.

The scattering function $F(\vec{r}_{N+1})$ is further expanded in the Kohn method in a combined basis of Gaussian (ϕ_i) and continuum (Ricatti-Bessel, j_l, and Hankel, h_l^+) basis functions:

$$F(\vec{r}) = \sum_i c_i \phi_i(\vec{r}) + \sum_{lm} [j_l(kr)\delta_{ll_0}\delta_{mm_0} + T_{ll_0mm_0} h_l^+(kr)]Y_{lm}(\hat{r})/r, \tag{3}$$

where $Y_{lm}(\hat{r})$ are spherical harmonics. Applying the stationary principle for the T matrix,

$$T_{\text{stat}} = T_{\text{trial}} - 2\int \Psi(H-E)\Psi, \tag{4}$$

results in a set of linear equations for the coefficients c_i, d_μ, and $T_{ll_0mm_0}$. The T-matrix elements $T_{ll_0mm_0}$ are the fundamental dynamical quantities from which all fixed-nuclei cross sections are derived.

B. Effective potential formalisms

Electron scattering calculations on polyatomics rapidly become computationally intensive as the number of target electrons increases. We therefore employed effective core potentials (ECP's) to aid with the computational efficiency. Effective core potentials were originally introduced to simplify electronic structure calculations by eliminating the need to rigorously describe the core electron states of heavy atoms. This can be justified under the assumption that many of the chemical and physical properties of molecules and materials are determined by the detailed correlation of outer-shell electrons, whereas the inner-shell electrons merely provide an average field for the valence electrons that is largely independent of the chemical environment in which the heavy atom is found.

In scattering studies, at energies low enough so that the incident electron does not possess sufficient energy to excite the core electrons, one expects the collision dynamics to be largely determined by the electron-valence target interactions and, hence, insensitive to the detailed behavior of the core electrons.

The procedures used to generate ECP's from all-electron atomic wave functions can be found elsewhere [11,12]. For this discussion, we begin with a solution of the atomic Hartree-Fock equations, which produces a set of orbitals that we partition into core, ϕ_c, and valence, ϕ_v, groups. According to the "shape-consistent" [13] prescription, the valence orbitals are replaced by pseudo-orbitals which are required to be identical to the true valence orbitals ϕ_v beyond some matching radius r_{match}. The effective potential U_l, which replaces the core-core and valence-core portions of the all-electron Fock Hamiltonian, is then defined by

$$U_l = \left[\left(\epsilon_v + \frac{1}{2}\frac{d^2}{dr^2} - \frac{l(l+1)}{2r^2} + \frac{Z^{\text{eff}}}{r} - W_{val}\right)\chi_v\right] \Big/ \chi_v, \tag{5}$$

where Z^{eff} is the effective nuclear charge (i.e., $Z^{\text{eff}} = Z - Z^{core}$) and W_{val} is the interaction potential (Coulomb plus exchange) between an electron in the valence pseudo-orbital, χ_v, and the electrons in other occupied pseudoorbitals. ϵ_v is the true orbital energy of the atomic Hartree-Fock orbital. By construction, the pseudo-orbital χ_v must be nodeless, guaranteeing that it is the lowest-energy eigenfunction and that Eq. (5) can be carried out for any $r > 0$.

The various l-dependent core potentials can be combined into a unified ECP for use in a molecular environment by using angular momentum projection operators:

$$U^{core} = U_L(r) + \sum_{l=0}^{L-1}\sum_{m=-l}^{l} [U_l(r) - U_L(r)]|lm\rangle\langle lm| \equiv U_L(r) + \sum_{l=0}^{L-1} \Delta U_l(r) P_l, \tag{6}$$

where L is 1 greater than the maximum value of l found among the core orbitals. This representation assumes that for angular momentum values greater than or equal to L, the core orbitals can be globally represented by a single, l-independent central potential $U_L(r)$, which provides the effect of Coulomb and exchange which are common to all valence electrons. The second term in Eq. (6) provides the repulsive parts of the core potential that are specific to each l value. Because of the projection operators introduced in Eq. (6), the ECP is a nonlocal operator.

The complex Kohn method uses numerical continuum functions, all defined about a single center, in the trial wave function and thus requires the numerical evaluation of

TABLE I. Gaussian basis sets used in e^--C_2F_4 scattering calculations. For symmetries $^2B_{1g}$, $^2B_{2g}$, $^2B_{1u}$, and $^2B_{2u}$ only those components of the diffuse scattering functions that contribute by symmetry were included in the calculation.

Center	Type	Exponent	Coefficient
Target basis			
Carbon	*s*	4.36200	1.00000
Carbon	*s*	1.50000	1.00000
Carbon	*s*	0.43660	1.00000
Carbon	*s*	0.17230	1.00000
Carbon	*s*	0.08716	1.00000
Carbon	*p*	6.78700	1.00000
Carbon	*p*	3.00000	1.00000
Carbon	*p*	1.49700	1.00000
Carbon	*p*	0.42970	1.00000
Carbon	*p*	0.12860	1.00000
Carbon	*d*	0.75000	1.00000
Fluorine	*s*	11.38000	1.00000
Fluorine	*s*	1.13200	1.00000
Fluorine	*s*	0.56250	1.00000
Fluorine	*s*	0.25660	1.00000
Fluorine	*p*	17.16000	1.00000
Fluorine	*p*	3.89300	1.00000
Fluorine	*p*	1.08800	1.00000
Fluorine	*p*	0.29800	1.00000
Fluorine	*p*	0.15000	1.00000
Fluorine	*d*	0.90000	1.00000
Diffuse scattering basis, ^2A_g symmetry			
Center of mass	*s*	0.04000	1.00000
Center of mass	*s*	0.05000	1.00000
Diffuse scattering basis, $^2B_{1g}$ and $^2B_{2g}$ symmetries			
Center of mass	*d*	0.30000	1.00000
Center of mass	*d*	0.15000	1.00000
Center of mass	*d*	0.08000	1.00000
Center of mass	*d*	0.04000	1.00000
Diffuse scattering basis, $^2B_{3g}$ symmetry			
Center of mass	*d*	0.30000	1.00000
Diffuse scattering basis, $^2B_{1u}$ and $^2B_{2u}$ symmetries			
Center of mass	*p*	0.70000	1.00000
Center of mass	*p*	0.50000	1.00000
Center of mass	*p*	0.20000	1.00000
Diffuse scattering basis, $^2B_{3u}$ symmetry			
Center of mass	*p*	0.50000	1.00000
Center of mass	*p*	0.20000	1.00000

bound-free and free-free matrix elements. Unfortunately, the nonlocal portion of U^{core} does not readily lend itself to numerical quadrature, since the angular projection operators are all defined about the various atomic centers. Rescigno and McCurdy [14] therefore reexpanded $\Delta U_l(r)P_l$ as a sum of separable terms using a product basis $|\alpha lm\rangle$, consisting of N radial functions multiplied by spherical harmonics, all centered on the atom in question:

$$\Delta U_l(r)P_l \approx \Delta U_l^{\text{sep}} = \sum_{\alpha,\beta=1}^{N} \sum_{m=-l}^{l} \Delta U_l|\alpha lm\rangle d^N_{\alpha,\beta}\langle \beta lm|\Delta U_l, \tag{7}$$

where the $d^N_{\alpha,\beta}$ are the radial elements of the matrix inverse

$$[d^{-1}]_{\alpha,\beta} = \langle \alpha|U_l - U_L|\beta\rangle. \tag{8}$$

With the expansion given by Eq. (7), matrix elements involving free functions will have the following form:

$$\langle f_\gamma|\Delta U_l^{\text{sep}}|f_\delta\rangle = \sum_{\alpha,\beta=1}^{N} \sum_{m=-l}^{l} \langle f_\gamma|\Delta U_l|\alpha lm\rangle d^N_{\alpha,\beta}\langle \beta lm|\Delta U_l|f_\delta\rangle. \tag{9}$$

In contrast to the work that would be required if the representation of Eq. (6) were used, the evaluation of the matrix elements required in Eq. (9) is straightforward. Further details about the theoretical formulation of effective potential methods in variational treatments of electron-molecule collisions can be found in Ref. [14].

III. THEORETICAL MODELS FOR ELECTRON-MOLECULE COLLISIONS: COMPUTATIONAL DETAILS AND RESULTS

The fixed-nuclei results we are reporting were all carried out for C_2F_4 at its equilibrium geometry (R_{CC} = 1.311 Å, R_{CF} = 1.319 Å, F-C-F = 112.48°). The target ground state was described by a self-consistent field (SCF) wave function. The carbon and fluorine 1*s* electrons were replaced by ECP's using the core potential parameters published by Pacios and Christiansen [15]. To compute the target SCF wave function we used the Gaussian basis sets, in uncontracted form, given by these authors, augmented with several additional functions. The molecular quadrupole moment obtained from the present calculation was −1.319454 a_0^2 To construct the trial wave function for the variational scattering calculations, the target basis was further augmented with additional diffuse Gaussian functions, depending on the symmetry in question. Table I lists the basis sets employed in all our scattering calculations. The expansion of the trial scattering function was completed by including numerically generated continuum basis functions, retaining terms with angular momentum quantum numbers l and $|m|$ less than or equal to 6.

In an approach similar to that employed in our study of C_2H_4 [8], we found that an accurate description of the low-energy scattering by C_2F_4 requires a proper treatment of the dominant physical processes in each symmetry. The following subsections will briefly describe the different approximations that were considered and how they were introduced into our calculations, and will show the individual symmetry components of the integral cross sections resulting from each of these approaches. Total elastic cross sections, momentum transfer cross sections, and angular differential cross sec-

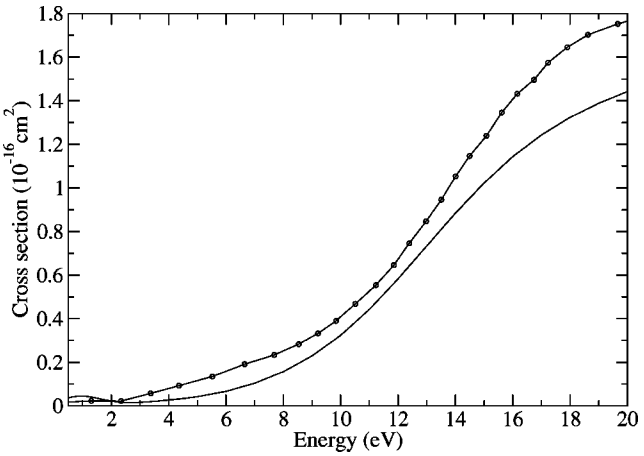

FIG. 1. $^2B_{1g}$ symmetry component of the integrated cross section. Solid curve: present calculations. Solid curve with circles: calculations by Winstead and McKoy [4]. Cross sections were calculated using the SE approximation.

tions, compared with experimental results and available theoretical calculations by Winstead and McKoy [4], will be presented in the last subsection.

A. Static exchange

The simplest approximation for describing an electron-molecule collision, consistent with the Pauli principle, is the so-called static-exchange (SE) appromixation in which the trial wave function is expressed as an antisymmetrized product of the target wave function and a scattered electron function, i.e., as the first term of Eq. (1). This model cannot be expected to yield accurate results at collision energies (generally less than 5 eV) where target polarization is important, at least for total symmetries in which the incident electron significantly penetrates the target, since it makes no allowance for the target to relax in the presence of the scattering electron. This model can describe shape resonances, although SE results generally place their position too high and their width too broad in energy.

The static-exchange approximation is a well-defined computational model and is therefore useful for establishing numerical convergence: indeed, different computational methods, if carried out to convergence, should all yield identical cross sections at the SE level. Moreover, in the absence of resonances or other specific low-energy features, the SE approximation will provide a useful description of the scattering process. We have treated the symmetry $^2B_{1g}$ using the SE approximation. The scattered electron wave function in $^2B_{1g}$ symmetry has a leading *d*-wave component and evidently does not penetrate the target significantly. The low-energy cross sections in this symmetry are small and display no resonance enhancement. Our calculated cross sections for this symmetry are shown in Fig. 1 along with the SE results of Winstead and McKoy [4]; the agreement is quite good.

B. Polarized SCF

At low incident electron energies, the collision cross sections can be sensitive to the effects of dynamic target electron polarization. Previous work on other closed-shell molecules has shown that including a set of specific configurations in Eq. (1) to produce what is known as a "polarized SCF" (PSCF) trial wave function provides a good description of target polarization, with a balance of correlation effects in the N- and $(N+1)$-electron systems [8,16–20]. In the PSCF approach [18] the CSF's Θ_μ, have a "two-particle, one-hole" structure since they are constructed as the product of bound virtual molecular orbitals and terms obtained by singly exciting the target SCF wave function into a subspace of unoccupied orbitals. Instead of using all the unoccupied orbitals to define the space of singly excited CSF's, we choose a compact subset of these virtual orbitals, the polarized virtual orbitals [ϕ_α in Eq. (2)], for singly exciting the target. There will, in general, be three polarized orbitals, one for each Cartesian component of the dipole operator, generated by each occupied orbital that is polarized. These polarized orbitals describe the linear response of the target to an externally applied electric field and are constructed following the prescription of Ref. [18].

The entire space of target and supplemental diffuse basis functions listed in Table I was used in the construction of the polarized orbitals. The target polarizability we obtained from a CI calculation that included all single excitations from the ground-state SCF wave function into the polarized orbitals was 27.56 a_0^3; we are not aware of an experimentally determined value of polarizability for C_2F_4.

In cases where the target molecule has a center of inversion, as it does here, the dipole operator only connects orbitals of opposite parity. Since there are occupied orbitals of both gerade and ungerade symmetries, the set of polarized orbitals in the present case spans all the irreducible representations of the point group D_{2h}. Therefore, the PSCF model, which includes terms generated by singly exciting an occupied orbital into the full set of polarized orbitals, will contain both dipole-allowed excitations, which describe long-range polarization, and excitations from an occupied orbital into orbitals of the same symmetry, which describe short-range relaxation. The latter class of excitations is important for the proper description of shape resonances.

We found that the cross sections in ^2A_g, $^2B_{3g}$, and $^2B_{3u}$ symmetries were dramatically lowered by including polarization terms in the trial wave function. Unfortunately, computational limitations prevented us from performing PSCF calculations using all 18 occupied orbitals and the full corresponding set of 54 polarized virtual orbitals. The maximum number of occupied orbitals we could employ in a full PSCF calculation was 14, so further approximations were tested. For the $^2B_{3g}$ and $^2B_{3u}$ symmetry cases, preliminary calculations carried out at the static-exchange level showed no evidence of shape resonances below 15 eV. This led us to believe that for these symmetries the cross sections would be most sensitive to long-range dipole-allowed excitations in the trial wave function. We therefore carried out PSCF calculations, using all 18 occupied orbitals, but restricted the space of target excitations to include only those where an occupied orbital was singly excited to polarized orbitals of opposite parity. These calculations were compared to full PSCF calculations using the 14 highest occupied orbitals. These two sets of calculations produced only small differences in the $^2B_{3g}$ and $^2B_{3u}$ cross sections.

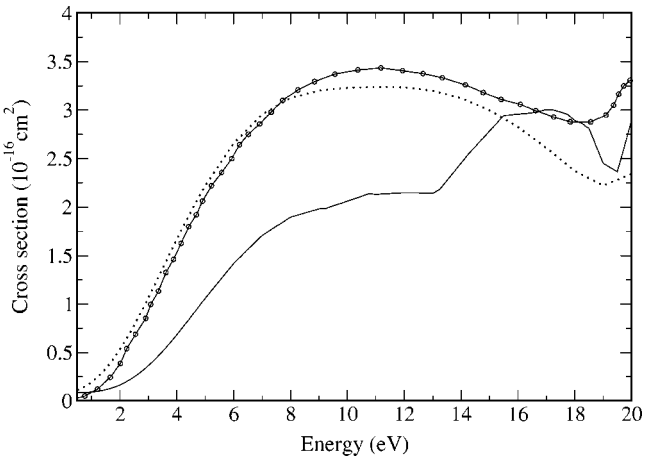

FIG. 2. $^2B_{3g}$ symmetry component of the integrated cross section. Cross sections were obtained by performing a PSCF calculation, having polarized the 14 highest occupied orbitals (solid curve). Dotted curve: SE calculations. Solid curve with circles: SE calculations by Winstead and McKoy [4].

The $^2B_{3g}$ cross sections are displayed in Fig. 2. At the static-exchange level, our results agree reasonably well with those of Winstead and McKoy [4]. Both calculations show evidence of a weak resonance near 20 eV, accompanied by a rapid rise in the eigenphase sum (not shown) near the upper limit of the energy range studied. Inclusion of polarization terms into the calculation is seen to lower the integrated cross sections below 15 eV by almost a factor of 2 and to shift the resonance to lower energy. Figure 3 shows the integrated cross sections in $^2B_{3u}$ symmetry. In this case, our static-exchange calculations produced cross sections somewhat smaller than those of Winstead and McKoy [4]. Once again, the inclusion of polarization terms into the trial function leads to a significant reduction in the magnitude of the integrated cross sections.

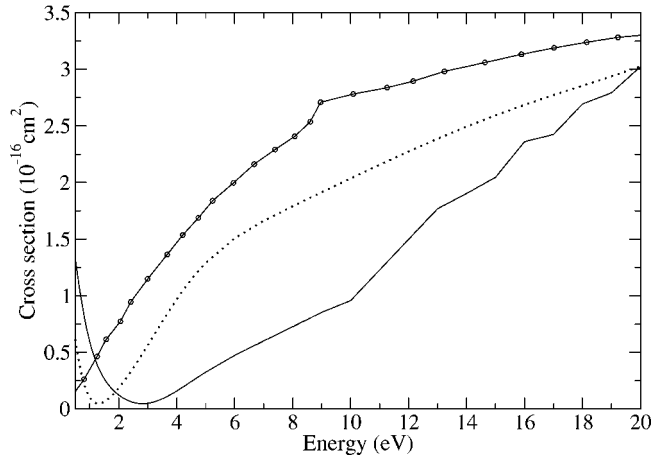

FIG. 3. $^2B_{3u}$ symmetry component of the integrated cross section. Cross sections were obtained from a PSCF calculation with polarized orbitals generated by allowed dipole transitions from all 18 occupied orbitals (solid curve). Dotted curve: SE calculations. Solid curve with circles: SE calculations by Winstead and McKoy [4].

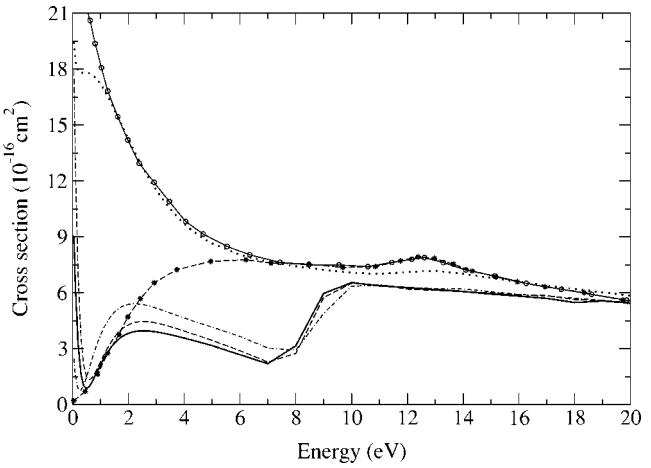

FIG. 4. ^2A_g symmetry component of the integrated cross section. Solid curve: polarization of 14 occupied orbitals including both allowed and forbidden dipole transitions. Chain curve: polarization of 18 occupied orbitals including only allowed dipole transitions. Dashed curve: polarization of 18 occupied orbitals including only allowed dipole transitions of the $C_2F_4^-$ negative ion. Dotted curve: SE calculations. Solid curve with circles: SE calculations by Winstead and McKoy [4]. Dashed curve with stars: adjusted calculations by Winstead and McKoy [4].

At this point, it is worth noting that the weak structures seen in the $^2B_{3u}$ cross section above 10 eV are associated with narrow pseudoresonances caused by the neglect of electronically open channels. The first electronically excited state of C_2F_4 is the $^3B_{1u}(T)$ state, which has a measured vertical excitation energy of 4.68 eV [21]. The corresponding singlet (V) state has a vertical excitation energy measured between 8.8 eV [21] and 8.9 eV [22]. The particular form of the trial function we used [Eq. (1)] approximates excited-state channels with discrete square-integrable terms (pseudostates) which in turn gives rise to spurious structures near pseudostate thresholds. These structures are typically narrow and are easily identified, so we can easily avoid them by choosing a grid of energies at which to plot the calculated cross sections.

In ^2A_g symmetry, the scattered electron can significantly penetrate the target and the cross sections in this symmetry are particularly sensitive to changes in the trial wave function. The static-exchange cross sections shown in Fig. 4, which agree very well with those of Winstead and McKoy [4], show a spurious *s*-wave enhancement below 4 eV, which is typical of calculations performed at this level. There is also the hint of a weak resonance near 12 eV. Including polarization terms in the trial wave function produces a pronounced resonance feature in the cross section near 9 eV, which was evidently obscured at the static-exchange level by the rapid rise in the low-energy cross section, as well as a Ramsauer-Townsend minimum. A series of PSCF calculations, including progressively more occupied orbitals in the generation of the polarized virtual orbitals, showed that the resonance feature and the magnitude of the cross sections above 8 eV were quick to converge. On the low-energy side of resonance, however, particularly near the local maximum near 2 eV, the cross sections were found to be more sensitive

to the number of occupied orbitals that were polarized. Calculations at energies below 0.5 eV confirmed the presence of a Ramsauer-Townsend minumum and are included in Fig. 4.

Because the ^2A_g cross sections display a shape resonance as well as a Ramsauer-Townsend minumum, scattering in this symmetry is expected to be sensitive to short-range distortion as well as long-range polarization. Indeed, a restricted PSCF calculation that employed all 18 occupied orbitals, but that only included dipole-allowed target excitations, produced cross sections, shown in Fig. 4, that were ~25% percent higher than an unrestricted PSCF using 14 occupied orbitals and that moved the resonance to higher energy. To verify the importance of short-range distortion effects in this symmetry, we performed a third set of calculations. We carried out an SCF calculation on the $C_2F_4^-$ anion in the target basis, using the neutral orbitals as a starting guess. The SCF iterations were found to stabilize after three iterations and the calculation was stopped. We then repeated the restricted (dipole-allowed) PSCF calculation with the 18 occupied "negative-ion" orbitals. As Fig. 4 shows, these results are reasonably close to the unrestricted PSCF calculations that used 14 occupied orbitals.

The cross sections that were finally included in our differential, total, and momentum-transfer cross sections calculations were the ones obtained from the variational calculations that included excitations into polarized orbitals generated using the 14 highest occupied orbitals with both dipole-allowed and -forbidden transitions. The polarizabilty obtained with this set of occupied orbitals was 26.97 a_0^3, which is 97.8% of the value obtained when all 18 occupied orbitals are included in the evaluation of the polarizability. By comparing the results of PSCF calculations that used different numbers of occupied orbitals in generating the correlation terms, we were able to determine an approximate scaling of the low-energy cross sections with polarizability. Based on this approximate scaling, we estimate that a PSCF calculation that included excitations from all 18 occupied orbitals would produce results in the 0–8 eV energy approximately 12% smaller than our 14 orbital PSCF calculation.

Also shown in Fig. 4 are the modified results of Winstead and McKoy [4], in which they included an *ad hoc* low-energy cutoff to eliminate the spurious *s*-wave enhancement found in the static-exchange cross sections. This adjustment, however, gives a ^2A_g cross section that differs markedly from our calculated results.

C. Relaxed SCF

The $^2B_{2g}$, $^2B_{2u}$, and $^2B_{1u}$ cross sections all display low-energy shape resonances. In such cases, short-range orbital relaxation effects dominate and it is important to strike a proper balance between correlation in the N- and $(N+1)$-electron systems. We have found that the PSCF model may lead to an unbalanced description of correlation in the temporary negative-ion state relative to the SCF target state at short range, with the result that the resonance will appear at too low an energy relative to the target ground state. Previous experience with a number of closed-shell target molecules [8,16,20,23–25] has shown that in such cases a "relaxed-SCF" (RSCF) model provides a good description of the scattering. The key is to include in the trial function only those correlation terms that produce an orbital relaxation effect, similar to the type of relaxation that would be produced by performing an SCF calculation on the negative ion. The relaxed-SCF trial function only includes configurations Θ_μ built from single excitations of the occupied target orbitals into virtual orbitals of the same symmetry; no $\phi_o \rightarrow \phi_\alpha$ excitation that breaks the spatial symmetry of the ground state is included in the calculation. This type of trial function describes the essential short-range core relaxation effects that are needed to describe a shape resonance but does not include the long-range dipole-polarization effects of the PSCF model. We therefore constructed a relaxed-SCF trial wave function for symmetries $^2B_{2g}$, $^2B_{2u}$, and $^2B_{1u}$. Winstead and McKoy [4] employed a similar model for these symmetries in their Schwinger variational calculations. The integral cross sections for these symmetries are shown in Figs. 5–7, along with the results of Winstead and McKoy [4]. There is evi-

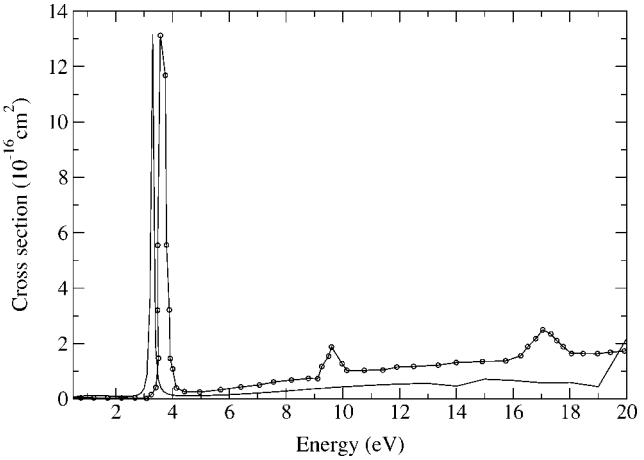

FIG. 5. $^2B_{2g}$ symmetry component of the integrated cross section. Solid curve: RSCF calculations. Solid curve with circles: calculations by Winstead and McKoy [4].

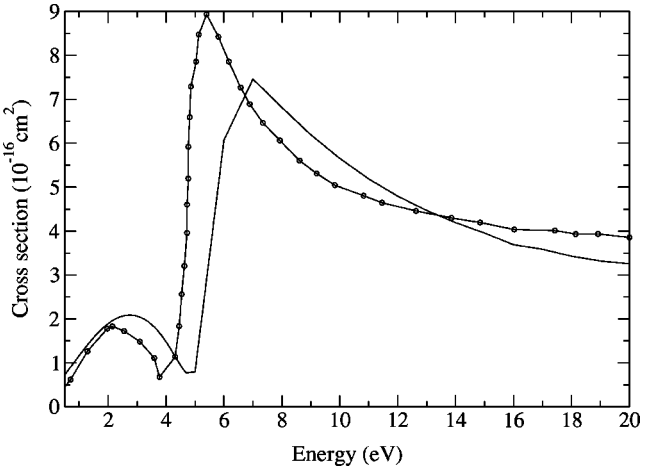

FIG. 6. $^2B_{2u}$ symmetry component of the integrated cross section. Solid curve: RSCF calculations. Solid curve with circles: calculations by Winstead and McKoy [4].

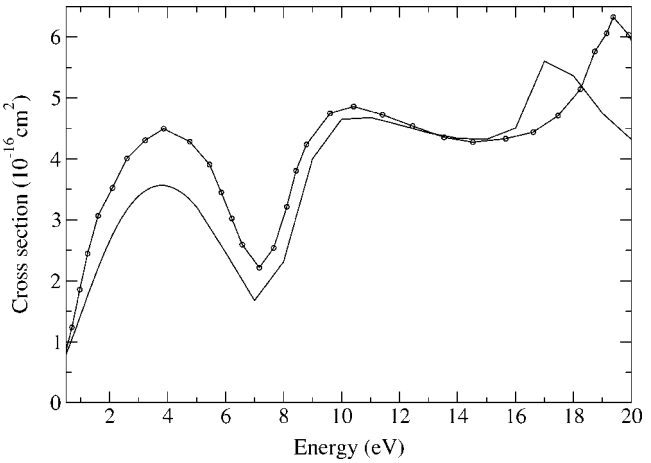

FIG. 7. $^2B_{1u}$ symmetry component of the integrated cross section. Solid curve: RSCF calculations. Solid curve with circles: calculations by Winstead and McKoy [4].

dently good agreement between the two sets of calculated cross sections.

The $^2B_{2g}$ cross section plotted in Fig. 5 shows a sharp resonance near 3.1 eV superimposed on a small nonresonant background. This is the π^* shape resonance, observed in electron transmission by Chiu *et al.* [26] at 3.0 eV. They measured the derivative of the transmitted electron current, but did not report cross sections, so a direct comparison with our calculated results is not possible. A similar feature was found in the case of C_2H_4 [8], although the resonance width at equilibrium geometry is an order of magnitude smaller in the present case. The $^2B_{2g}$ resonance position is expected to depend strongly on geometry. Such a narrow resonance, when averaged over vibrational motion, is considerably broadened and may not give rise to a sharp feature in the elastic cross section. The π^* resonance does play an important role in dissociative electron attachment [27] and would be expected to lead to strong vibrational excitation.

Other resonance features, present in symmetries $^2B_{2u}$ and $^2B_{1u}$, can be seen in Figs. 6 and 7, respectively. The $^2B_{2u}$ cross section, plotted in Fig. 6, shows a pronounced resonance feature near 5.5 eV. Unlike the $^2B_{2g}$ π^* resonance, which displays a pure Breit-Wigner form, the $^2B_{2u}$ resonance is accompanied by a strong energy-dependent background which gives the cross section a highly asymmetric profile. Winstead and McKoy's calculations produced a similar result, with a resonance position roughly 1 eV lower than the present result. In contrast to the narrow π^* resonance, the broader $^2B_{2u}$ resonance would be expected to be readily observable in the total cross section, even after vibrational motion were taken into account.

The $^2B_{1u}$ cross sections are plotted in Fig. 7. There are evidently two shape resonances in this symmetry. These were confirmed by rapid rises in the eigenphase sum near 8 eV and near 17 eV. These resonances again occur in the presence of a strong, energy-dependent background, which is responsible for the broad peak near 4 eV. Our calculations in this symmetry are in good agreement with the results of Winstead and McKoy.

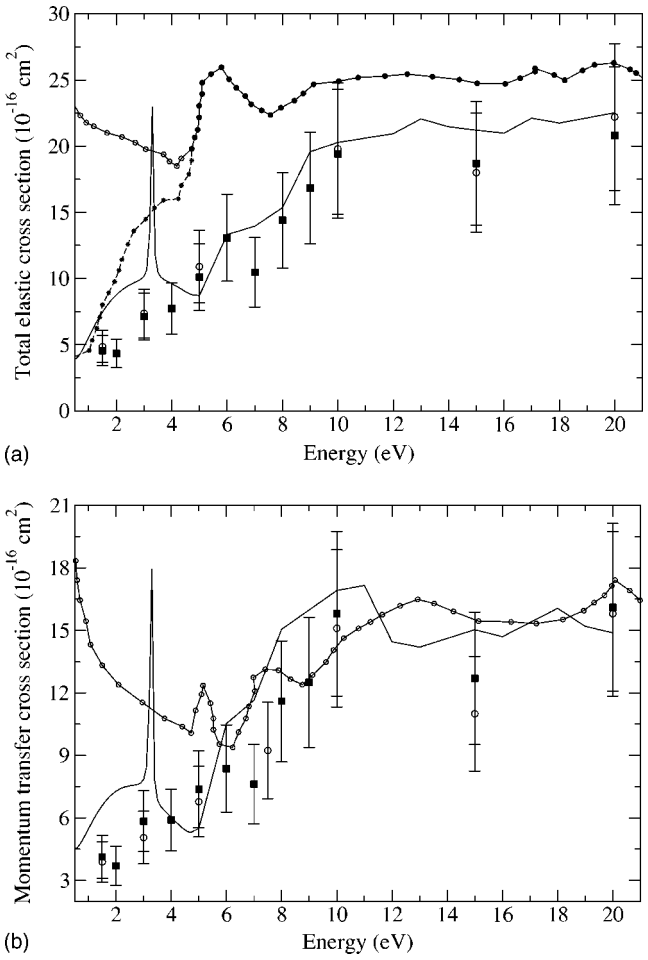

FIG. 8. Total elastic and momentum-transfer cross sections for e-C_2F_4 scattering. Solid curves: present results. Solid curves with circles: calculations by Winstead and McKoy [4]. Dashed curves with stars: adjusted calculations by Winstead and McKoy [4]. Open circles: ANU measurements by Panajotovic *et al.* [6]. Squares: Sophia measurements by Panajotovic *et al.* [6].

D. Total and differential cross sections

The results of fixed-nuclei calculations in different total symmetries, all carried out at the target equilibrium geometry, were combined to produce total (vibrationally summed) elastic cross sections, momentum-transfer cross sections, and angular differential cross sections for incident electron energies between 0.5 and 20 eV. As explained above, the PSCF model was used for symmetries ^2A_g, $^2B_{3g}$, and $^2B_{3u}$, while symmetries $^2B_{2g}$, $^2B_{1u}$, and $^2B_{2u}$ were treated with an RSCF approach. Symmetry $^2B_{1g}$, which makes a very small contribution to the cross sections at low energies, was treated at the static-exchange level. Symmetry ^2A_u is unimportant over the energy range considered here and was left out of the calculations.

The total elastic and momentum-transfer cross sections are plotted in Fig. 8 The experimental values were obtained by Panajotovic *et al.* [6] on two different crossed-beam electron spectrometers: open circles refer to measurements at the Australian National University (ANU), while squares represent measurements performed at Sophia University, Japan

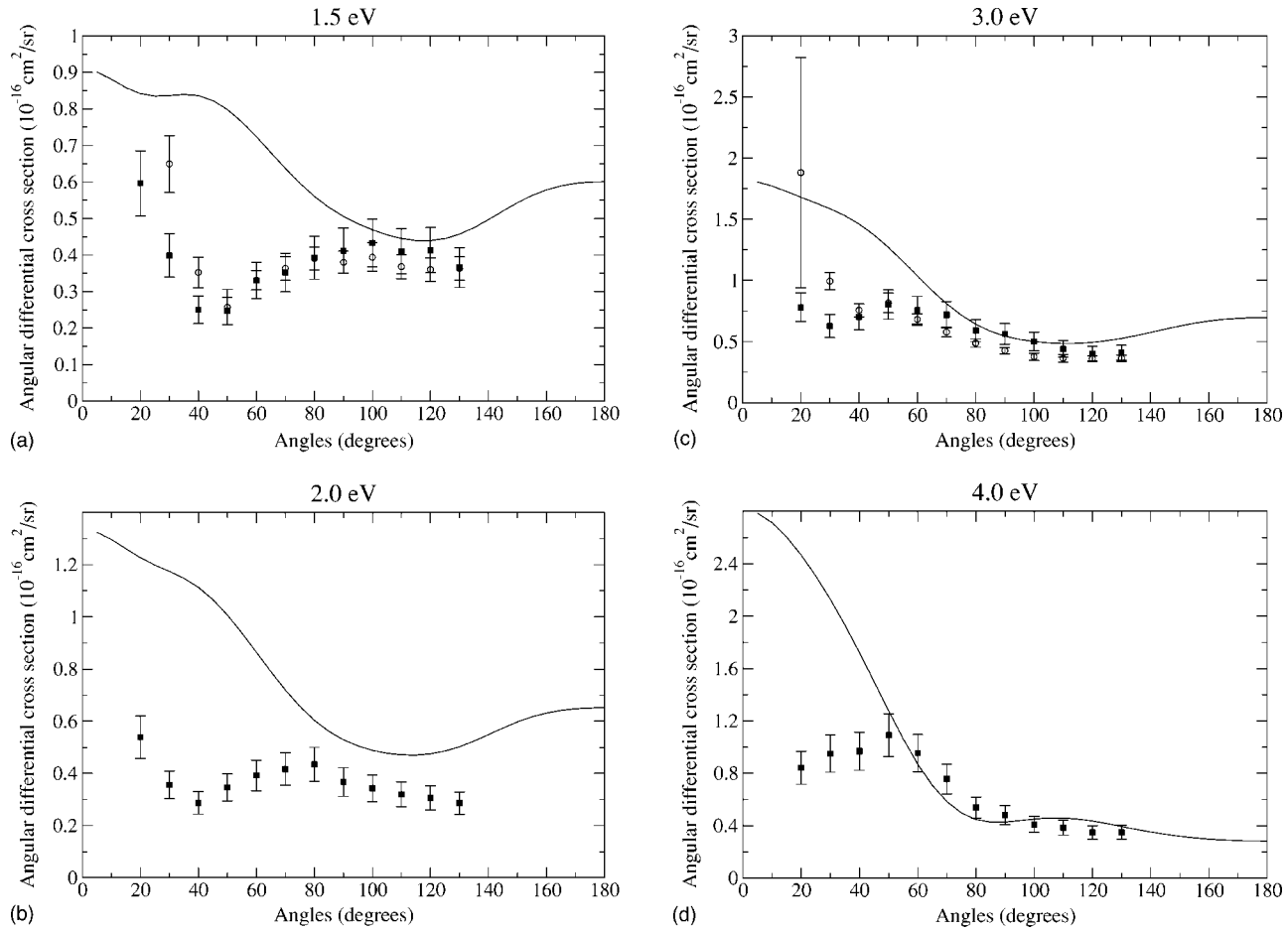

FIG. 9. Elatic differential cross sections for e-C_2F_4 scattering at incident energies *4* eV and below. Solid curves: present results. Solid curves with circles: calculations by Winstead and McKoy [4]. Open circles: ANU measurements by Panajotovic *et al.* [6]. Squares: Sophia measurements by Panajotovic *et al.* [6].

(Sophia). The calculated total and momentum transfer cross sections are in relatively good agreement with experiment at energies above 4 eV. The rapid rise in the calculated cross sections near 5 eV, which is associated with the $^2B_{2u}$ resonance, is also evident in the measured cross sections, which show a peak between 5 and 7 eV, although more data points would be needed to resolve this structure. Below 4 eV, our calculated cross sections are somewhat larger than the measured values. A more exhaustive inclusion of polarization effects, particularly in the ^2A_g and $^2B_{1u}$ symmetry components, is evidently needed at these lower energies to obtain quantitative agreement with experiment. There is no evidence of the sharp π^* resonance, which appears prominantly in the fixed-nuclei calculations, for reasons discussed above. The results of Winstead and McKoy [4] are also plotted in Fig. 8. Their total integrated cross sections are uniformly larger than our calculated values. Their momentum transfer cross sections were only calculated at the static-exchange level and therefore display qualitatively incorrect low-energy behavior.

Figures 9 and 10 show elastic angular differential cross sections at different incident electron energies. Again, the experimental measurements are those of Panajotovic *et al.* Above 4 eV, there is very good agreement between our calculated values and experiment. Winstead and McKoy [4] reported differential cross sections at 10 and 15 eV, computed at the static-exchange level, and these are also plotted in Fig. 10. Their cross sections are substantially larger than our results at small scattering angles (note the log scale in Fig. 10), but are in better aggrement at large scattering angles.

Below 4 eV, our calculated cross sections agree less well with experiment, particularly at scattering angles less than 40° where they are uniformly too large. It is worth noting, however, that there appear to be systematic differences between the ANU and Sophia measurements at small scattering angles. These differences are particularly large at 1.5 and 3.0 eV. We observed a similar trend in the case of C_2H_2 [28] and, as in the case of ethylene, the present calculations are in better agreement with the ANU measurements. Unfortunately, at 2.0 and 4.0 eV, we only have the Sophia measurements for comparison and our cross sections appear to significantly overestimate experiment at small angles. We have previously mentioned that calculations in this energy range are very sensitive to polarization effects, particularly in the penetrating ^2A_g, $^2B_{1u}$, and $^2B_{2u}$ symmetries, and a more exhaustive treatment is evidently required at these low energies.

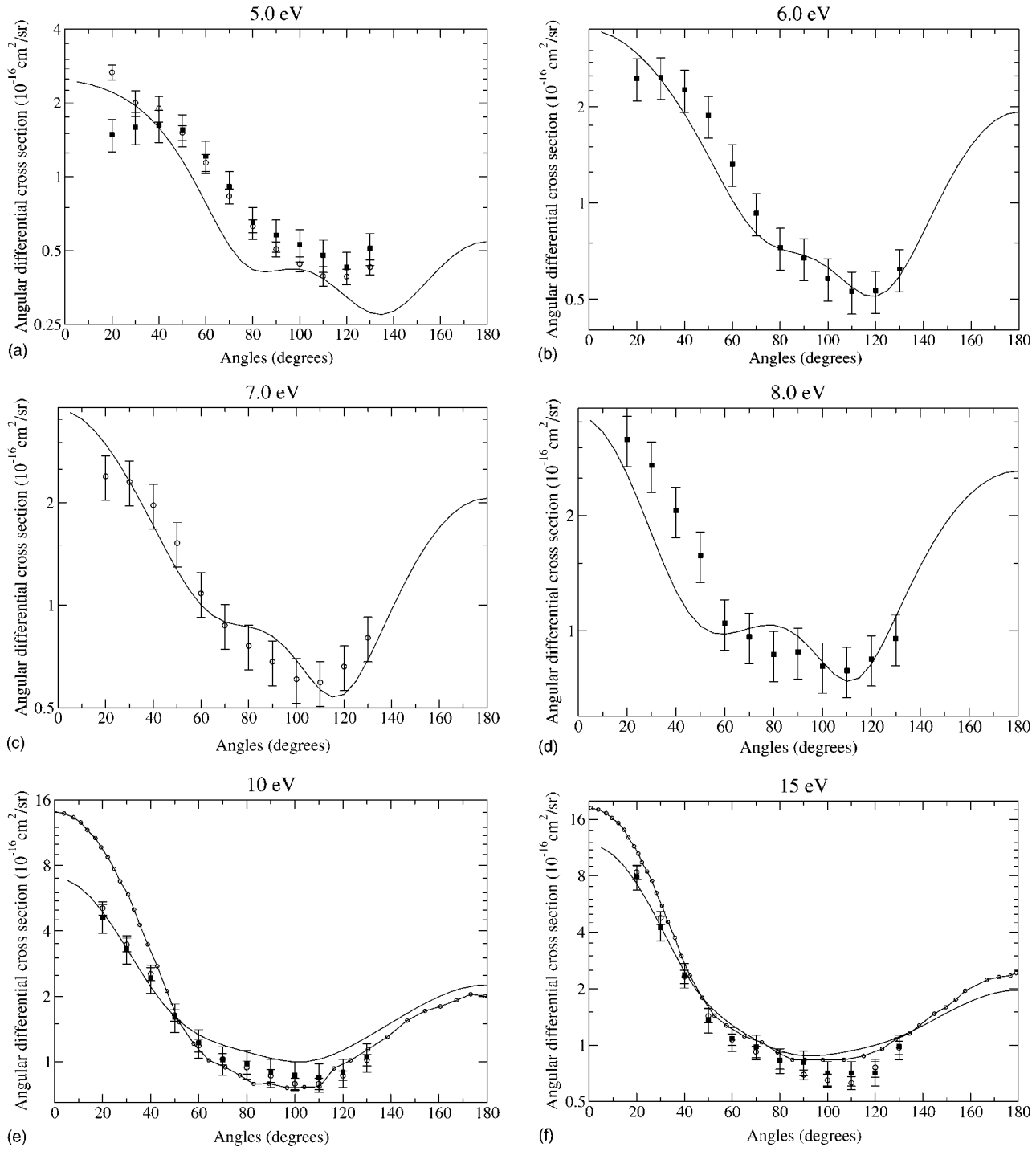

FIG. 10. Elastic differential cross sections for e-C_2F_4 scattering at incident energies above 4 eV. Solid curves: present results. Solid curves with circles: calculations by Winstead and McKoy [4]. Open circles: ANU measurements by Panajotovic *et al.* [6]. Squares: Sophia measurements by Panajotovic *et al.* [6].

IV. CONCLUSIONS

We have carried out a variational treatment of electronically elastic e^--C_2F_4 scattering. Effective core potentials were introduced into the calculations to eliminate the need to treat the carbon and fluorine 1*s* electrons explicitly and to make the computations more tractable The agreement we find, at the static-exchange level, with previous all-electron calculations of Winstead and McKoy [4], indicates that there are no significant errors introduced by using ECP's. Dynamic correlation and polarization effects were introduced into the calculations at different levels of approximation. A polarized-SCF approach was used for symmetries ^2A_g, $^2B_{3g}$, and $^2B_{3u}$, while in $^2B_{2g}$, $^2B_{1u}$, and $^2B_{2u}$ symmetries, where there are low-energy shape resonances, we employed a relaxed-SCF model.

We find good agreement with recent experiment, in both integrated and differential electronically elastic cross sections, at energies above 4 eV. Below 4 eV, where the calculated results are extremely sensitive to polarization effects, we find larger differences, particularly in the differential cross sections at small scattering angles, as present code limitations prevented us from carrying out a more extensive set of calculations. Low-energy electron scattering by target molecules of this size represent a formidable challenge for *ab initio* theory. The use of effective core potentials can help make the calculations more tractable, but more work will be needed to obtain quantitatively accurate cross sections at collision energies of a few electron volts.

ACKNOWLEDGMENTS

This work was performed under the auspices of the U. S. Department of Energy by the University of California Lawrence Berkeley National Laboratory. The work was supported by the U. S. DOE Office of Basic Energy Science, Division of Chemical Sciences. A.E.O. acknowledges support from the National Science Foundation (Grant No. PHY-99-87877). We are grateful to C. W. McCurdy for helpful discussions.

[1] S. Samukawa, T. Mukai, and K. Tsuda, J. Vac. Sci. Technol. A **17**, 2551 (1999).
[2] S. Samukawa and T. Mukai, Thin Solid Films **374**, 235 (2000).
[3] S. Samukawa, T. Mukai, and Noguchi, Mater. Sci. Semicond. Process. **2**, 203 (1999).
[4] C. Winstead and V. McKoy, J. Chem. Phys. **116**, 1380 (2002).
[5] K. Yoshida, S. Goto, H. Tagashira, C. Winstead, V. McKoy, and W. L. Morgan, J. Appl. Phys. **91**, 2637 (2002).
[6] R. Panajotovic, M. Jelisavcic, R. Kajita, T. Tanaka, M. Kitajima, H. Cho, H. Tanaka, and S. J. Buckman, J. Chem. Phys. (to be published).
[7] R. Kajita, M. Jelisavcic, M. Kitajima, R. Panajotovic, S. Eden, H. Tanaka, H. Cho, and S. J. Buckman, International Symposium on Electron-Molecule Collisions and Swarms, Program and Abstracts, 2003, Prague, Czech Republic (unpublished).
[8] C. S. Trevisan, A. E. Orel, and T. N. Rescigno, Phys. Rev. A **68**, 062707 (2003).
[9] T. N. Rescigno, C. W. McCurdy, A. E. Orel, and B. H. Lengsfield, in *Computational Methods for Electron-Molecule Collisions*, edited by W. M. Huo and F. A. Gianturco (Plenum, New York, 1995).
[10] T. N. Rescigno, B. H. Lengsfield, and C. W. McCurdy, in *Modern Electronic Structure Theory*, edited by D. R. Yarkony (World Scientific, Singapore, 1995), Vol. 1.
[11] L. R. Kahn, P. Baybutt, and D. G. Truhlar, J. Chem. Phys. **65**, 3826 (1976).
[12] G. B. Bachelet, D. R. Hamann, and M. Schlüter, Phys. Rev. B **26**, 4199 (1982).
[13] P. A. Christiansen, Y. S. Lee, and K. S. Pitzer, J. Chem. Phys. **71**, 4445 (1979).
[14] T. N. Rescigno and C. W. McCurdy, J. Chem. Phys. **104**, 120 (1995).
[15] L. F. Pacios and P. A. Christiansen, J. Chem. Phys. **82**, 2664 (1985).
[16] B. I. Schneider, T. N. Rescigno, B. H. Lengsfield, and C. W. McCurdy, Phys. Rev. Lett. **66**, 2728 (1991).
[17] T. N. Rescigno, D. A. Byrum, W. A. Isaacs, and C. W. McCurdy, Phys. Rev. A **60**, 2186 (1999).
[18] B. H. Lengsfield, T. N. Rescigno, and C. W. McCurdy, Phys. Rev. A **44**, 4296 (1991).
[19] W. A. Isaacs, C. W. McCurdy, and T. N. Rescigno, Phys. Rev. A **58**, 309 (1998).
[20] W. A. Isaacs, C. W. McCurdy, and T. N. Rescigno, Phys. Rev. A **58**, 2881 (1998).
[21] M. J. Coggiola, W. M. Flicker, O. A. Mosher, and A. Kuppermann, J. Chem. Phys. **65**, 2655 (1976).
[22] G. Bélanger and C. Sandorfy, J. Chem. Phys. **55**, 2055 (1971).
[23] B. I. Schneider and L. A. Collins, Phys. Rev. A **30**, 95 (1984).
[24] A. U. Hazi, T. N. Rescigno, and M. Kurilla, Phys. Rev. A **23**, 1089 (1981).
[25] T. N. Rescigno, C. W. McCurdy, and B. I. Schneider, Phys. Rev. Lett. **63**, 248 (1989).
[26] N. S. Chiu, P. D. Burrow, and K. K. Jordan, Chem. Phys. Lett. **68**, 121 (1979).
[27] M. Heni, E. Illenberger, H. Baumgärtel, and S. Süzer, Chem. Phys. Lett. **87**, 244 (1982).
[28] R. Panajotovic, M. Kitajima, H. Tanaka, M. Jelisavcic, J. Lower, L. Campbell, M. J. Brunger, and S. J. Buckman, J. Phys. B **36**, 1615 (2003).